Zeitschrift: IABSE publications = Mémoires AIPC = IVBH Abhandlungen
Band: 34 (1974)

Artikel: Discrete analysis of curved slab-beam systems
Autor: Buragohain, D.N. / Agrawal, S.B.
DOI: https://doi.org/10.5169/seals-26281

Nutzungsbedingungen
Die ETH-Bibliothek ist die Anbieterin der digitalisierten Zeitschriften auf E-Periodica. Sie besitzt keine Urheberrechte an den Zeitschriften und ist nicht verantwortlich für deren Inhalte. Die Rechte liegen in der Regel bei den Herausgebern beziehungsweise den externen Rechteinhabern. Das Veröffentlichen von Bildern in Print- und Online-Publikationen sowie auf Social Media-Kanälen oder Webseiten ist nur mit vorheriger Genehmigung der Rechteinhaber erlaubt. Mehr erfahren

Conditions d'utilisation
L'ETH Library est le fournisseur des revues numérisées. Elle ne détient aucun droit d'auteur sur les revues et n'est pas responsable de leur contenu. En règle générale, les droits sont détenus par les éditeurs ou les détenteurs de droits externes. La reproduction d'images dans des publications imprimées ou en ligne ainsi que sur des canaux de médias sociaux ou des sites web n'est autorisée qu'avec l'accord préalable des détenteurs des droits. En savoir plus

Terms of use
The ETH Library is the provider of the digitised journals. It does not own any copyrights to the journals and is not responsible for their content. The rights usually lie with the publishers or the external rights holders. Publishing images in print and online publications, as well as on social media channels or websites, is only permitted with the prior consent of the rights holders. Find out more

Download PDF: 02.01.2026

ETH-Bibliothek Zürich, E-Periodica, https://www.e-periodica.ch

Discrete Analysis of Curved Slab-Beam Systems

Analyse discrète de systèmes courbes de poutres en té

Diskrete Analyse gekrümmter Plattenbalken-Systeme

D. N. BURAGOHAIN
Ph. D., Assistant Professor

S. B. AGRAWAL
Research Scholar, Department of Civil Engineering, Indian Institute of Technology, Bombay, India

1. Introduction

The analysis of curved slab-beam systems has received the attention of structural analysts for more than a decade particularly with reference to curved girder bridges. However, a realistic analysis of curved slabs monolithic with eccentric beams in circumferential and radial directions has become possible only with the development of modern analytical techniques requiring the use of digital computers.

Four essentially different approximate techniques have been used. The first approach due to SAWKO [1] replaces the plate and beam structure by an equivalent grillage of intersecting beams whose stiffnesses are adjusted to approximate those of the slab and beams. The second approach, used by HEINS and HAILS [2], treats the curved plate-beam system as an equivalent polar orthotropic plate. However, the determination of the torsional rigidity of the equivalent orthotropic plate and the evaluation of plate and beam forces in the final results remain the major problems in this approach. The third approach is the application of the slope-deflection Fourier series method, as used by BELL and HEINS [3], to analyse continuous orthotropic slabs on flexible curved girders.

A fourth approach is to analyse the curved slab-beam system as a curved thin-walled beam of open section [4]. However, this approach cannot be generally used as it is based on the assumption that the cross-section as a whole retains its original shape during deformation. In the first three approaches it is difficult to separate the slab and beam forces when the beams

are integral with and eccentric to the slab, and the shear lag effect is not considered. The determination of the effective flange width of the composite beams also requires considerable judgement when the beams are not closely spaced. The need for the use of a more efficient and realistic method like the finite element technique has been discussed by GUSTAFSON and WRIGHT [5] who applied this technique to straight and skewed composite girder bridges. DAVIES et al. [6] later applied the finite element method to curved girder bridges. The added advantage of the finite element method is that it can be applied to a curved slab-beam system in general, not necessarily a bridge, with any boundary conditions. The aim of this paper is to report the developments and application of an equally efficient method to curved slab-beam systems.

The development of a discrete energy approach for polar orthotropic curved plates has been earlier reported by BURAGOHAIN [7]. The same approach is extended to curved slab-beam systems considering both bending and in-plane forces and displacements. The total potential energy of the slab is discretized into energy due to extension and bending and energy due to shear and twisting, contributed by corresponding tributary elements, and the minimization procedure yields the corresponding element matrices. Similar formulations are obtained for the eccentric circumferential and radial beams. For the particular case of repetitive radial beams closely spaced at equal intervals, an orthotropic plate formulation is presented in which the stiffnesses of the slab and radial beams are merged together with due consideration of the eccentricity of the beams.

Results are presented for three numerical examples consisting of a straight five girder composite I-beam bridge, a curved slab model with four longitudinal and eleven radial beams, and a two span two girder curved bridge model.

2. Method of Analysis

A section of a curved slab-beam system is shown in Fig. 1, wherein the forces and displacements at the middle plane of the slab and at the centroidal axes of the longitudinal and radial beams are indicated along with the coordinate directions (r, Φ, z). The discrete energy formulation for the slab-beam system is presented in three parts: for slab, for longitudinal beams, and for radial beams.

2.1. Polar Orthotropic Slab Analysis

A segment of the curved slab between any two longitudinal beams is discretized using a modified finite difference scheme, shown in Fig. 2, separately into two sets of tributary areas, designated as Class A and Class B elements,

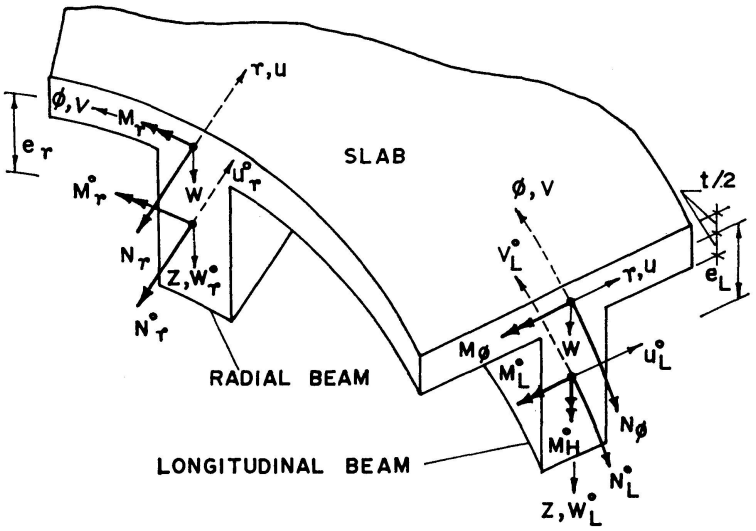

Fig. 1. Curved slab with eccentric beams.

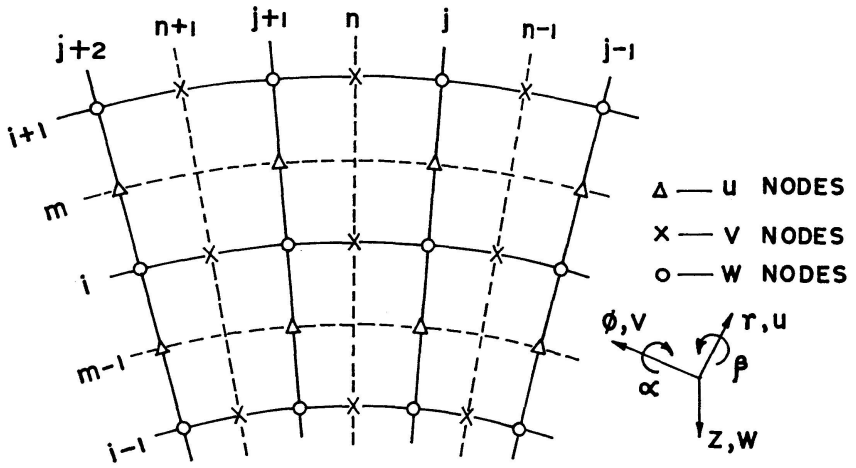

Fig. 2. Nodal layout for slab.

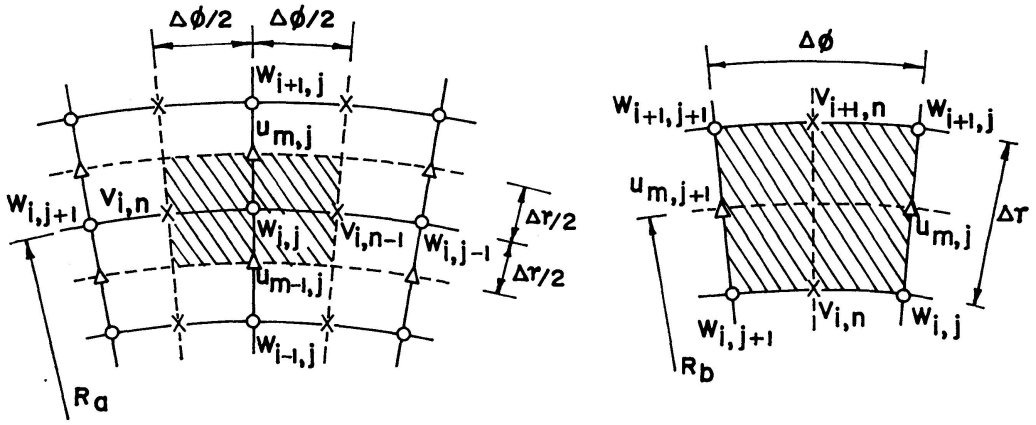

a) Class A element b) Class B element

Fig. 3. Element discretization for slab.

for considering energy due to extension and bending and energy due to shear and twisting respectively. Fig. 3 shows these two classes of elements with reference to the nodal layout. The potential energy π_a for Class A elements and π_b for Class B elements are considered separately.

Class A elements: The strain vector $\{\epsilon_a^s\}$ for class A elements of the slab consists of the membrane strains ϵ_r^s and ϵ_Φ^s and the curvatures k_r^s and k_Φ^s at the slab middle surface, given by:

$$\{\epsilon_a^s\} = \begin{Bmatrix} \epsilon_r^s \\ \epsilon_\Phi^s \\ k_r^s \\ k_\Phi^s \end{Bmatrix} = \begin{Bmatrix} \dfrac{\partial u}{\partial r} \\ \dfrac{u}{r} + \dfrac{\partial v}{r\,\partial \Phi} \\ -\dfrac{\partial^2 w}{\partial r^2} \\ -\left(\dfrac{1}{r}\dfrac{\partial w}{\partial r} + \dfrac{\partial^2 w}{r^2\,\partial \Phi^2}\right) \end{Bmatrix}. \tag{1}$$

Referring to Fig. 3a, Eq. (1) may be expressed in finite difference form as:

$$\{\epsilon_a^s\} = \begin{Bmatrix} \dfrac{1}{\Delta r}(u_{m,j} - u_{m-1,j}) \\ \dfrac{1}{2R_a}(u_{m,j} + u_{m-1,j}) + \dfrac{1}{R_a \Delta \Phi}(v_{i,n} - v_{i,n-1}) \\ -\dfrac{1}{\Delta r^2}(w_{i+1,j} - 2w_{i,j} + w_{i-1,j}) \\ -\left(\dfrac{w_{i+1,j} - w_{i-1,j}}{2R_a \Delta r} + \dfrac{w_{i,j+1} - 2w_{i,j} + w_{i,j-1}}{R_a^2 \Delta \Phi^2}\right) \end{Bmatrix}, \tag{2}$$

or, symbolically,

$$\{\epsilon_a^s\} = [B_a^s]\{\delta_a^s\}, \tag{3}$$

in which

$$[B_a^s] = \begin{bmatrix} \dfrac{1}{\Delta r} & \dfrac{-1}{\Delta r} & 0 & 0 & 0 & 0 & 0 & 0 & 0 \\ \dfrac{1}{2R_a} & \dfrac{1}{2R_a} & \dfrac{1}{R_a \Delta \Phi} & \dfrac{-1}{R_a \Delta \Phi} & 0 & 0 & 0 & 0 & 0 \\ 0 & 0 & 0 & 0 & \dfrac{2}{\Delta r^2} & \dfrac{-1}{\Delta r^2} & \dfrac{-1}{\Delta r^2} & 0 & 0 \\ 0 & 0 & 0 & 0 & \dfrac{2}{R_a^2 \Delta \Phi^2} & \dfrac{-1}{2R_a \Delta r} & \dfrac{1}{2R_a \Delta r} & \dfrac{-1}{R_a^2 \Delta \Phi^2} & \dfrac{-1}{R_a^2 \Delta \Phi^2} \end{bmatrix} \tag{4}$$

and $\{\delta_a^s\}$ is the element displacement vector, given by

$$\{\delta_a^s\}^T = \{u_{m,j}\, u_{m-1,j}\, v_{i,n}\, v_{i,n-1}\, w_{i,j}\, w_{i+1,j}\, w_{i-1,j}\, w_{i,j+1}\, w_{i,j-1}\}. \tag{5}$$

The stress resultants $\{N_a^s\}$ for class A elements at slab middle surface consist of the in-plane forces N_r^s and N_Φ^s and the bending moments M_r^s and M_Φ^s in radial and tangential directions respectively. Using polar orthotropic theory, the stress resultants may be expressed in terms of the strain components as:

$$\{N_a^s\} = \begin{Bmatrix} N_r^s \\ N_\Phi^s \\ M_r^s \\ M_\Phi^s \end{Bmatrix} = [D_a^s]\{\epsilon_a^s\} = [D_a^s][B_a^s]\{\delta_a^s\}, \tag{6}$$

in which

$$[D_a^s] = \begin{bmatrix} C_{rr}t & C_{r\Phi}t & 0 & 0 \\ C_{\Phi r}t & C_{\Phi\Phi}t & 0 & 0 \\ 0 & 0 & \dfrac{C_{rr}t^3}{12} & \dfrac{C_{r\Phi}t^3}{12} \\ 0 & 0 & \dfrac{C_{\Phi r}t^3}{12} & \dfrac{C_{\Phi\Phi}t^3}{12} \end{bmatrix}. \tag{7}$$

In Eq. (7), t is the thickness of the slab, and if E_r, μ_r and E_Φ, μ_Φ are the modulii of elasticity and Poisson's ratios associated with the coordinate directions, then

$$\begin{aligned} C_{rr} &= \frac{E_r}{1-\mu_r\mu_\Phi}, \qquad C_{\Phi\Phi} = \frac{E_\Phi}{1-\mu_r\mu_\Phi}, \\ C_{r\Phi} &= \frac{\mu_\Phi E_r}{1-\mu_r\mu_\Phi} = \frac{\mu_r E_\Phi}{1-\mu_r\mu_\Phi} = C_{\Phi r}. \end{aligned} \tag{8}$$

For an isotropic slab, $E_r = E_\Phi = E$ and $\mu_r = \mu_\Phi = \mu$.

The potential energy π_a^s of the class A element of the slab is then obtained as:

$$\begin{aligned} \pi_a^s = &\int_0^{\Delta\Phi}\int_0^{\Delta r} \tfrac{1}{2}\{\delta_a^s\}^T[B_a^s]^T[D_a^s][B_a^s]\{\delta_a^s\} - \{\delta_a^s\}^T\{Q\}\,r\,dr\,d\Phi = \\ &\tfrac{1}{2}\{\delta_a^s\}^T[B_a^s]^T[D_a^s][B_a^s]\{\delta_a^s\}\,R_a\Delta r\Delta\Phi - \{\delta_a^s\}^T\{Q\}\,R_a\Delta r\Delta\Phi, \end{aligned} \tag{9}$$

in which

$$\{Q\}^T = \{0\ 0\ 0\ 0\ p_z\ 0\ 0\ 0\ 0\} \tag{10}$$

and p_z = uniformly distributed load intensity in z direction.

Class B elements: The strain vector $\{\epsilon_b^s\}$ for class B elements of the slab consists of the membrane shearing strain $\gamma_{r\Phi}^s$ and the twisting curvature $k_{r\Phi}^s$ given by:

$$\{\epsilon_b^s\} = \begin{Bmatrix} \gamma_{r\Phi}^s \\ k_{r\Phi}^s \end{Bmatrix} = \begin{Bmatrix} \dfrac{\partial u}{r\,\partial\Phi} + \dfrac{\partial v}{\partial r} - \dfrac{v}{r} \\ 2\left(\dfrac{\partial^2 w}{r\,\partial r\,\partial\Phi} - \dfrac{\partial w}{r^2\,\partial\Phi}\right) \end{Bmatrix}. \tag{11}$$

Referring to Fig. 3b, Eq. (11) may be expressed in finite difference form as:

$$\{\epsilon_b^s\} = \begin{Bmatrix} \dfrac{u_{m,j+1}-u_{m,j}}{R_b \Delta\Phi} + \dfrac{v_{i+1,n}-v_{i,n}}{\Delta r} - \dfrac{v_{i+1,n}+v_{i,n}}{2R_b} \\ 2\left(\dfrac{w_{i+1,j+1}-w_{i+1,j}+w_{i,j}-w_{i,j+1}}{R_b \Delta r \Delta\Phi} - \dfrac{w_{i+1,j+1}+w_{i,j+1}}{2R_b^2 \Delta\Phi} + \dfrac{w_{i+1,j}+w_{i,j}}{2R_b^2 \Delta\Phi}\right) \end{Bmatrix} \quad (12)$$

or symbolically, $$\{\epsilon_b^s\} = [B_b^s]\{\delta_b^s\}, \quad (13)$$

in which $\{\delta_b^s\}$ is the element displacement vector, given by

$$\{\delta_b^s\}^T = \{u_{m,j+1}\, u_{m,j}\, v_{i+1,n}\, v_{i,n}\, w_{i+1,j+1}\, w_{i,j}\, w_{i+1,j}\, w_{i,j+1}\} \quad (14)$$

and

$$[B_b^s] = \begin{bmatrix} \dfrac{1}{R_b \Delta\Phi} & \dfrac{-1}{R_b \Delta\Phi} & (c-d) & (-c-d) & 0 & 0 & 0 & 0 \\ 0 & 0 & 0 & 0 & (e-f) & (-e-f) & (f-e) & (e+f) \end{bmatrix}, \quad (15)$$

in which $$c = \frac{1}{\Delta r},\ d = \frac{1}{2R_b},\ e = \frac{-1}{R_b^2 \Delta\Phi} \text{ and } f = \frac{-2}{R_b \Delta r \Delta\Phi}. \quad (16)$$

The stress resultants $\{N_b^s\}$ for class B elements at slab middle surface consist of the membrane shear force $N_{r\Phi}^s$ and the twisting moment $M_{r\Phi}^s$, which can be expressed using polar orthotropic theory as:

$$\{N_b^s\} = \begin{Bmatrix} N_{r\Phi}^s \\ M_{r\Phi}^s \end{Bmatrix} = [D_b^s]\{\epsilon_b^s\} = [D_b^s][B_b^s]\{\delta_b^s\}, \quad (17)$$

in which $$[D_b^s] = \begin{bmatrix} G_{r\Phi} t & 0 \\ 0 & \dfrac{G_{r\Phi} t^3}{12} \end{bmatrix}, \quad (18)$$

in which $G_{r\Phi}$ = shear modulus of elasticity.

The potential energy π_b^s for class B elements of the slab is then given by:

$$\pi_b^s = \int_0^{\Delta\Phi}\int_0^{\Delta r} \tfrac{1}{2}\{\delta_b^s\}^T [B_b^s]^T [D_b^s][B_b^s]\{\delta_b^s\} - \{\delta_b^s\}^T\{P\}\, r\, dr\, d\Phi = \tfrac{1}{2}\{\delta_b^s\}^T [B_b^s]^T [D_b^s][B_b^s]\{\delta_b^s\}\, R_b \Delta r \Delta\Phi - \{\delta_b^s\}^T\{P\}\, R_b \Delta r \Delta\Phi, \quad (19)$$

in which $$\{P\}^T = \left\{\frac{p_r}{2}\ \frac{p_r}{2}\ \frac{p_\Phi}{2}\ \frac{p_\Phi}{2}\ 0\ 0\ 0\ 0\right\} \quad (20)$$

and p_r and p_Φ are uniformly distributed surface load intensities in r and Φ directions respectively.

Overall Stiffness Matrix: The total potential energy for the slab is obtained as:

$$\pi^s = \sum_{n_a} \pi_a^s + \sum_{n_b} \pi_b^s, \quad (21)$$

in which n_a and n_b denote the number of class A and class B elements respectively.

Substituting Eqs. (9) and (19) in Eq. (21), the condition $\delta \pi^s = 0$ yields:

$$\sum_{n_a} (R_a \Delta r \Delta \Phi [B_a^s]^T [D_a^s] [B_a^s] \{\delta_a^s\} - R_a \Delta r \Delta \Phi \{Q\}) + \sum_{n_b} (R_b \Delta r \Delta \Phi [B_b^s]^T [D_b^s] [B_b^s] \{\delta_b^s\} - R_b \Delta r \Delta \Phi \{P\}) = 0. \tag{22}$$

Eq. (22) may be symbolically represented in a more familiar form as:

$$[K^s]\{\delta^s\} = \{f^s\}, \tag{23}$$

in which $\{\delta^s\}$ = overall displacement vector, $[K^s]$ = overall stiffness matrix, given by

$$[K^s] = \sum_{n_a} [K_a^s] + \sum_{n_b} [K_b^s] \tag{24}$$

and $\{f^s\}$ = overall load vector, given by

$$\{f^s\} = \sum_{n_a} \{f_a^s\} + \sum_{n_b} \{f_b^s\} + \{f_c^s\}. \tag{25}$$

In Eq. (24), $[K_a^s]$ and $[K_b^s]$ are respectively the class A and class B element matrices, given by

$$[K_a^s] = R_a \Delta r \Delta \Phi [B_a^s]^T [D_a^s] [B_a^s], \qquad [K_b^s] = R_b \Delta r \Delta \Phi [B_b^s]^T [D_b^s] [B_b^s]. \tag{26}$$

In Eq. (25), $\{f_a^s\}$ and $\{f_b^s\}$ are respectively the class A and class B element load vectors, given by

$$\{f_a^s\} = R_a \Delta r \Delta \Phi \{Q\}, \qquad \{f_b^s\} = R_b \Delta r \Delta \Phi \{P\} \tag{27}$$

and $\{f_c^s\}$ = load vector due to concentrated loads corresponding to appropriate nodal displacements.

Boundary Elements: Depending on its position along the boundaries, the class A element has eight other forms, denoted by A_2 through A_9, as shown in Fig. 4, when the pivotal node (i, j) lies on the boundary. In order to express the strains $\{\epsilon_a^s\}$ in terms of displacements within the region, the displacement u and the rotation $\alpha\left(= \frac{\partial w}{\partial r}\right)$ are introduced at node (i, j) at the boundary r = constant, and the displacement v and the rotation $\beta\left(= \frac{\partial w}{r \partial \Phi}\right)$ are introduced at node (i, j) at the boudary Φ = constant. Table 1 gives the finite difference expressions for the various terms in $\{\epsilon_a^s\}$ required for the boundary elements A_2 through A_9. The relation matrix $[B_a^s]$ and the element displacement vector $\{\delta_a^s\}$ are modified accordingly. The elemental area $R_a \Delta r \Delta \Phi$ is changed into $R_a \Delta r \Delta \Phi/2$ for elements A_2, A_3, A_4 and A_5 and into $R_a \Delta r \Delta \Phi/4$ for elements A_6, A_7, A_8 and A_9.

Stress Resultants: Once the overall displacement vector $\{\delta^s\}$ is obtained from the solution of Eq. (23), the element displacement vector $\{\delta_a^s\}$ or $\{\delta_b^s\}$ can be formed for each class A or class B element. The appropriate stress resultants are then computed at nodes (i, j) for class A elements and at nodes (m, n) for class B elements using Eqs. (6) and (17).

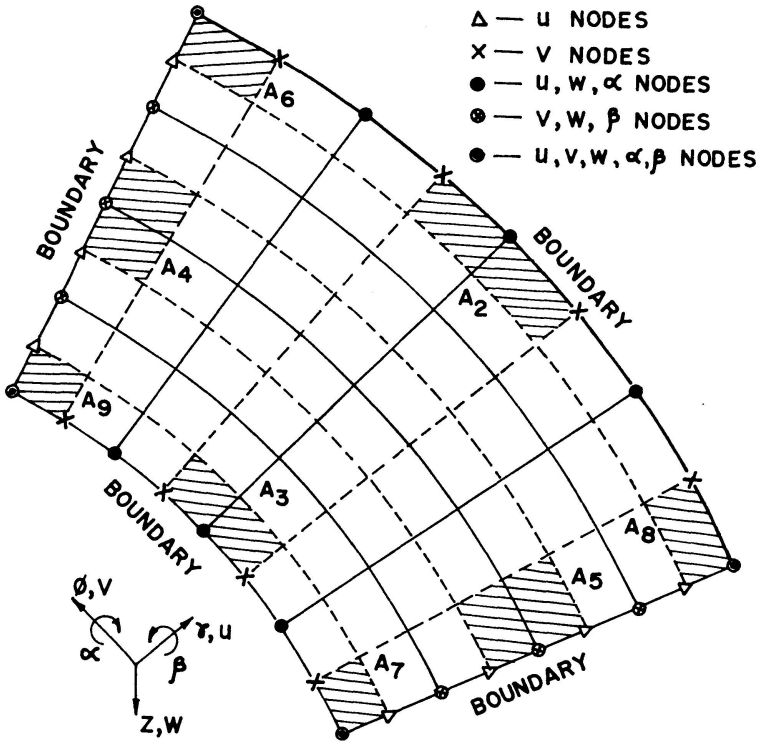

Fig. 4. Boundary elements and boundary nodes.

Table 1. Finite Difference Expressions for Different Terms of Strain Components Modified for Boundary Elements (see Fig. 4)

Terms	Finite difference expressions	
	elements A_2, A_6, A_8 [1])	elements A_3, A_7, A_9 [1])
$\frac{\partial u}{\partial r}$	$\frac{2(u_{i,j}-u_{m-1,j})}{\Delta r}$	$\frac{2(u_{m,j}-u_{i,j})}{\Delta r}$
$\frac{\partial^2 w}{\partial r^2}$	$\frac{2(\Delta r\,\alpha_{i,j}-w_{i,j}+w_{i-1,j})}{\Delta r^2}$	$\frac{2(w_{i+1,j}-w_{i,j}-\Delta r\,\alpha_{i,j})}{\Delta r^2}$
$\frac{\partial w}{r\partial r}$	$\frac{\alpha_{i,j}}{R_a}$	$\frac{\alpha_{i,j}}{R_a}$
	elements A_4, A_6, A_9 [1])	elements A_5, A_7, A_8 [1])
$\frac{\partial v}{r\partial \Phi}$	$\frac{2(v_{i,j}-v_{i,n-1})}{R_a\Delta\Phi}$	$\frac{2(v_{i,n}-v_{i,j})}{R_a\Delta\Phi}$
$\frac{\partial^2 w}{r^2\partial\Phi^2}$	$\frac{2(R_a\Delta\Phi\,\beta_{i,j}-w_{i,j}+w_{i,j-1})}{R_a^2\Delta\Phi^2}$	$\frac{2(w_{i,j+1}-w_{i,j}-R_a\Delta\Phi\,\beta_{i,j})}{R_a^2\Delta\Phi^2}$
	elements $A_2, A_3, A_6, A_7, A_8, A_9$ [1])	
$\frac{u}{r}$	$\frac{u_{i,j}}{R_a}$	

[1]) For elements not mentioned against a term, the expression for the term is the same as used in equation (2).

2.2. *Eccentric Curved Beam*

It is assumed that both radial and curved beams act monolithically with the slab and the breadth of the curved beam is assumed to be small in comparison with the radius. The junction of the slab with a longitudinal beam is taken as a boundary for the slab. Hence the displacements considered at the junction at the level of slab middle surface have to be related to the corresponding displacements at the centroid of the beam.

Element Discretization: The nodal breakdown for a curved beam is shown in Fig. 5a. The class A and class B beam elements are shown in Figs. 5b and 5c.

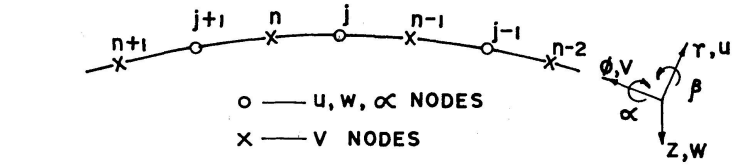

a) Nodal layout

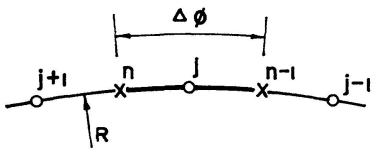

b) Class A element

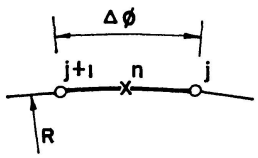

c) Class B element

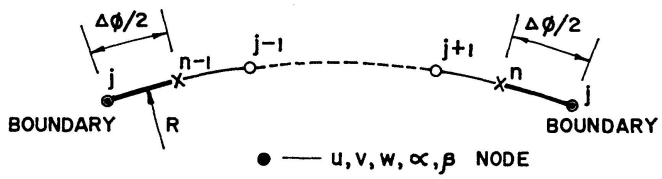

d) Boundary elements

Fig. 5. Nodal layout and elements for longitudinal beam.

Class A elements: The displacements at the junction of slab and beam at the level of slab middle-surface are u, v, w and α, which are related to the displacements at the centroid of the beam as (see Fig. 1):

$$\begin{aligned} u_L^0 &= u - e_L \frac{\partial w}{\partial r} = u - e_L \alpha, \\ v_L^0 &= v - e_L \frac{\partial w}{R \partial \Phi}, \qquad w_L^0 = w, \end{aligned} \tag{28}$$

in which R is the radius of the curved beam.

The strain vector $\{\epsilon_a^L\}$ for class A elements of the longitudinal curved beams consists of the axial strain ϵ_Φ^0 and curvatures in the vertical and horizontal planes, k_Φ^0 and k_H^0 respectively, given by

$$\{\epsilon_a^L\} = \begin{Bmatrix} \epsilon_\Phi^0 \\ k_\Phi^0 \\ k_H^0 \end{Bmatrix} = \begin{Bmatrix} \dfrac{u_L^0}{R} + \dfrac{dv_L^0}{R\,d\Phi} \\ -\left(\dfrac{\alpha}{R} + \dfrac{d^2 w}{R^2\,d\Phi^2}\right) \\ -\left(\dfrac{u_L^0}{R^2} + \dfrac{d^2 u_L^0}{R^2\,d\Phi^2}\right) \end{Bmatrix}. \tag{29}$$

Using the relations of Eq. (28), Eq. (29) may be written as:

$$\{\epsilon_a^L\} = \begin{Bmatrix} \dfrac{u}{R} + \dfrac{dv}{R\,d\Phi} - e_L\left(\dfrac{\alpha}{R} + \dfrac{d^2 w}{R^2\,d\Phi^2}\right) \\ -\left(\dfrac{\alpha}{R} + \dfrac{d^2 w}{R^2\,d\Phi^2}\right) \\ -\left(\dfrac{u}{R^2} + \dfrac{d^2 u}{R^2\,d\Phi^2}\right) + e_L\left(\dfrac{\alpha}{R^2} + \dfrac{d^2\alpha}{R^2\,d\Phi^2}\right) \end{Bmatrix}. \tag{30}$$

Referring to Fig. 5b, Eq. (30) may be represented using finite difference as:

$$\{\epsilon_a^L\} = \begin{Bmatrix} \dfrac{u_j}{R} + \dfrac{v_n - v_{n-1}}{R\,\Delta\Phi} - e_L\left(\dfrac{\alpha_j}{R} + \dfrac{w_{j+1} - 2w_j + w_{j-1}}{R^2\,\Delta\Phi^2}\right) \\ -\left(\dfrac{\alpha_j}{R} + \dfrac{w_{j+1} - 2w_j + w_{j-1}}{R^2\,\Delta\Phi^2}\right) \\ -\left(\dfrac{u_j}{R^2} + \dfrac{u_{j+1} - 2u_j + u_{j-1}}{R^2\,\Delta\Phi^2}\right) + e_L\left(\dfrac{\alpha_j}{R^2} + \dfrac{\alpha_{j+1} - 2\alpha_j + \alpha_{j-1}}{R^2\,\Delta\Phi^2}\right) \end{Bmatrix} \tag{31}$$

or symbolically

$$\{\epsilon_a^L\} = [B_a^L]\{\delta_a^L\}, \tag{32}$$

in which

$$\{\delta_a^L\}^T = \{u_j\, u_{j+1}\, u_{j-1}\, v_n\, v_{n-1}\, w_j\, w_{j+1}\, w_{j-1}\, \alpha_j\, \alpha_{j+1}\, \alpha_{j-1}\} \tag{33}$$

and

$$[B_a^L] = \begin{bmatrix} \dfrac{1}{R} & 0 & 0 & d & -d & 2ce_L & -ce_L & -ce_L & \dfrac{-e_L}{R} & 0 & 0 \\ 0 & 0 & 0 & 0 & 0 & 2c & -c & -c & -\dfrac{1}{R} & 0 & 0 \\ \left(2c - \dfrac{1}{R^2}\right) & -c & -c & 0 & 0 & 0 & 0 & 0 & \left(-2ce_L + \dfrac{e_L}{R^2}\right) & ce_L & ce_L \end{bmatrix}, \tag{34}$$

in which

$$c = \frac{1}{R^2\,\Delta\Phi^2}, \qquad d = \frac{1}{R\,\Delta\Phi}. \tag{35}$$

In Eq. (33), the displacement vector represents displacements at the slab middle surface.

If warping restraint is considered for the curved longitudinal beam, the torsion-bending curvature

$$-\left(\frac{d^2\alpha}{R^2\,d\Phi^2}-\frac{d^2w}{R^3\,d\Phi^2}\right)$$

is added as a fourth component in the strain vector $\{\epsilon_a^L\}$ and expressed in finite difference form in Eq. (31).

The stress resultants $\{N_a^L\}$ for class A beam element at the beam centroidal axis consist of the axial force N_L^0, the tangential moment M_L^0 and the horizontal moment M_H^0 and are expressed in terms of the strain components as:

$$\{N_a^L\}=\begin{Bmatrix}N_L^0\\M_L^0\\M_H^0\end{Bmatrix}=[D_a^L]\{\epsilon_a^L\}=[D_a^L][B_a^L]\{\delta_a^L\},\tag{36}$$

in which

$$[D_a^L]=\begin{bmatrix}E_L A_L & 0 & 0\\ 0 & E_L I_r^0 & 0\\ 0 & 0 & E_L I_z^0\end{bmatrix}.\tag{37}$$

In Eq. (37), E_L = modulus of elasticity for the beam, I_r^0 and I_z^0 are the moments of inertia about the beam centroidal axes in r and z directions respectively, and A_L is the cross-sectional area.

For considering warping, the torsion-bending bimoment is added as a fourth term in Eq. (36) and the warping rigidity $E_L I_w$ in Eq. (37), I_w being the sectorial moment of inertia for the beam.

Class B elements: For the class B beam element, the strain vector $\{\epsilon_b^L\}$ consists only of the twisting curvature $k_{r\Phi}^L$, given by:

$$\{\epsilon_b^L\}=\{k_{r\Phi}^L\}=\left\{\frac{d\alpha}{R\,d\Phi}-\frac{dw}{R^2\,d\Phi}\right\}.\tag{38}$$

Referring to Fig. 5c, Eq. (38) may be expressed in terms of displacements as:

$$\{\epsilon_b^L\}=\left\{\frac{\alpha_{j+1}-\alpha_j}{R\,\Delta\Phi}-\frac{w_{j+1}-w_j}{R^2\,\Delta\Phi}\right\}=[B_b^L]\{\delta_b^L\},\tag{39}$$

in which the displacement vector is

$$\{\delta_b^L\}^T=\{w_{j+1}\,w_j\,\alpha_{j+1}\,\alpha_j\}\tag{40}$$

and

$$[B_b^L]_{1\times 4}=\left[\frac{-1}{R^2\,\Delta\Phi}\;\frac{1}{R^2\,\Delta\Phi}\;\frac{1}{R\,\Delta\Phi}\;\frac{-1}{R\,\Delta\Phi}\right].\tag{41}$$

The twisting moment T_L is the only stress resultant and is related to $\{\epsilon_b^L\}$ as

$$\{N_b^L\}=\{T_L\}=[D_b^L]\{\epsilon_b^L\}=[D_b^L][B_b^L]\{\delta_b^L\},\tag{42}$$

in which

$$[D_b^L]=[G_L J_L].\tag{43}$$

In Eq. (43), G_L is the modulus of rigidity and J_L is the St. Venant torsional constant for the longitudinal beam.

Following the procedure described for the slab, the class A beam element matrix $[K_a^L]$ and the class B beam element matrix $[K_b^L]$ are obtained as:

$$[K_a^L] = R\Delta\Phi[B_a^L]^T[D_a^L][B_a^L], \qquad [K_b^L] = R\Delta\Phi[B_b^L]^T[D_b^L][B_b^L]. \quad (44)$$

These matrices for all class A and class B beam elements are added to the appropriate places of the overall stiffness matrix of the slab before solving the matrix Eq. (23). The stress resultants for the beam centroidal axes are obtained using Eqs. (36) and (43).

Boundary elements for beam: There will be two boundary elements for the beam as shown in Fig. 5d, when the pivotal node j lies on the boundary. Displacement v and rotation $\beta\left(=\frac{dw}{R\,d\Phi}\right)$ are introduced at the boundary nodes and the procedure followed is similar to that in the case of slab. In order to express the strain component k_H^0, two additional rotations $\theta_1\left(=\frac{du}{R\,d\Phi}\right)$ and $\theta_2\left(=\frac{d\alpha}{R\,d\Phi}\right)$ have to be introduced at the boundary node thus making a total of seven displacements at the node. However, except in the case of free boundary, the introduction of additional displacements may be avoided by using actual boundary conditions for the beam. For instance, for simply supported conditions, $\{\epsilon_a^L\}=0$ for the boundary elements.

2.3. Closely Spaced Eccentric Radial Beams

The formulation developed for the longitudinal beams may be followed also for the radial beams with the additional assumption that the radial beams are perfectly flexible normal to their planes. In this case, the junction of the radial beam with the slab will be treated as a boundary for the slab thus introducing additional displacements at these junctions. This can be avoided if the radial beams are of identical sections and are closely and equally spaced, in which case, the slab together with the radial beams is treated as a polar orthotropic slab in which the effect of eccentricity is duly considered. In this case, only the longitudinal beams form additional boundaries for the slab besides the four outer boundaries. Additional stiffnesses are then contributed by the radial beams to the class A and class B slab elements.

Class A element: Referring to Fig. 1, the displacements and strains at the centroid of the radial beams may be expressed in terms of the corresponding quantities at slab middle surface as:

$$w_r^0 = w, \qquad u_r^0 = u - e_r\frac{\partial w}{\partial r},$$

$$\epsilon_r^0 = \frac{du_r^0}{dr} = \frac{\partial u}{\partial r} - e_r\frac{\partial^2 w}{\partial r^2} = \epsilon_r^s + e_r k_r^s \quad (45)$$

and

$$k_r^0 = -\frac{\partial^2 w_r^0}{\partial r^2} = -\frac{\partial^2 w}{\partial r^2} = k_r^s.$$

In matrix form

$$\begin{Bmatrix} \epsilon_r^0 \\ k_r^0 \end{Bmatrix} = \begin{bmatrix} 1 & 0 & e_r & 0 \\ 0 & 0 & 1 & 0 \end{bmatrix} \begin{Bmatrix} \epsilon_r^s \\ \epsilon_\Phi^s \\ k_r^s \\ k_\Phi^s \end{Bmatrix} = [Z_r]\{\epsilon_a^s\}. \tag{46}$$

The forces in the radial beam at the level of centroidal axes are:

$$\begin{Bmatrix} N_r^0 \\ M_r^0 \end{Bmatrix} = \begin{bmatrix} E_r A_r & 0 \\ 0 & E_r I_\Phi^0 \end{bmatrix} \begin{Bmatrix} \epsilon_r^0 \\ k_r^0 \end{Bmatrix} = [D_a^r] \begin{Bmatrix} \epsilon_r^0 \\ k_r^0 \end{Bmatrix} = [D_a^r][Z_r]\{\epsilon_a^s\}, \tag{47}$$

in which, E_r is the modulus of elasticity, A_r is the cross-sectional area and I_Φ^0 is the moment of inertia about the centroidal horizontal axis for the radial beam. Transferring the centroidal forces of the beam to the level of the slab middle surface, and denoting these transferred forces as N_r^r and M_r^r,

$$N_r^r = N_r^0, \qquad M_r^r = e_r N_r^0 + M_r^0. \tag{48}$$

Denoting by $\{N_a^r\}$ the stress-resultants at slab middle surface due to the radial beams, for class A elements,

$$\{N_a^r\} = \begin{Bmatrix} N_r^r \\ N_\Phi^r \\ M_r^r \\ M_\Phi^r \end{Bmatrix} = \begin{bmatrix} 1 & 0 \\ 0 & 0 \\ e_r & 1 \\ 0 & 0 \end{bmatrix} \begin{Bmatrix} N_r^0 \\ M_r^0 \end{Bmatrix} = [Z_r]^T \begin{Bmatrix} N_r^0 \\ M_r^0 \end{Bmatrix} = [Z_r]^T [D_a^r][Z_r]\{\epsilon_a^s\}. \tag{49}$$

If the radial beams are uniformly spaced at angular interval Φ_s, the total internal forces per unit length $\{N_a\}$ at the level of (r, Φ, z) reference due to both slab and radial beams acting together will be:

$$\{N_a\} = \{N_a^s\} + \frac{1}{R_a \Phi_s}\{N_a^r\} = [D_a]\{\epsilon_a^s\} = [D_a][B_a^s]\{\delta_a^s\}, \tag{50}$$

in which
$$[D_a] = [D_a^s] + \frac{1}{R_a \Phi_s}[Z_r]^T [D_a^r][Z_r]. \tag{51}$$

The expression for the class A element matrix in Eq. (26) is then modified as:

$$[K_a] = R_a \Delta r \Delta \Phi [B_a^s]^T [D_a][B_a^s]. \tag{52}$$

Class B elements: The twist β and the twisting curvature $k_{r\Phi}^r$ of the radial beam are related to the corresponding quantities at the slab middle surface as:

$$\beta = \frac{\partial w}{r\,\partial \Phi}, \qquad k_{r\Phi}^r = \frac{\partial \beta}{\partial r} = \frac{\partial^2 w}{r\,\partial r\,\partial \Phi} - \frac{\partial w}{r^2\,\partial \Phi} = \tfrac{1}{2} k_{r\Phi}^s \tag{53}$$

and the twisting moment T_r of the radial beam is given by

$$T_r = G_r J_r k_{r\Phi}^r = \tfrac{1}{2} G_r J_r k_{r\Phi}^s, \tag{54}$$

in which G_r and J_r denote respectively the modulus of rigidity and the St. Venant torsional constant for the radial beam. The twisting moment due to radial beam equivalent to the slab twisting moment $M^s_{r\Phi}$ may be denoted as $M^r_{r\Phi}$. Since T_r represents twisting in one direction only, whereas both $M_{r\Phi}$ and $M_{\Phi r}$ for the slab are represented by $M^s_{r\Phi}$,

$$M^r_{r\Phi} = \tfrac{1}{2} T_r = \frac{G_r J_r}{4} k^s_{r\Phi}. \tag{55}$$

The total forces per unit length due to both slab and radial beams taken together are denoted as $\{N_b\}$, given by

$$\{N_b\} = [D_b]\{\epsilon^s_b\} = [D_b][B^s_b]\{\delta^s_b\}, \tag{56}$$

in which

$$[D_b] = \begin{bmatrix} G_{r\Phi} t & 0 \\ 0 & \left(\frac{G_{r\Phi} t^3}{12} + \frac{G_r J_r}{4 R_b \Phi_s}\right) \end{bmatrix}. \tag{57}$$

The expression for the class B element matrix in Eq. (26) is then modified as:

$$[K_b] = R_b \Delta r \Delta \Phi [B^s_b]^T [D_b][B^s_b]. \tag{58}$$

If the strains at the slab middle surface are known at a radial beam location, the forces at the centroid of the beam may be obtained using Eqs. (47) and (54).

3. Numerical Examples

The discrete energy method presented herein has been applied to three numerical examples and the results are compared with available theoretical and experimental values. Solutions for several mesh patterns for the same example, generally used to establish convergence, are not presented here; but it has been shown earlier [7] that the method generally gives upperbound values of deflections which converge towards the true solutions with finer discretizations.

Example 1: The first example is a 60 ft. span composite I-beam bridge, the cross-sectional properties of which are shown in Fig. 6. The solutions for this straight bridge are obtained by using infinite radius ($R = 10^{10}$ ft.) in the present method. Moment coefficients C_m, given by $M = C_m P a$, where M is the longitudinal moment in a composite beam, P is the applied load and "a" is the span, are compared with two sets of available solution and shown in Table 2. The first set of results was obtained by VITOLS et al. [8] by the exact solution of differential equations for a refined orthotropic theory in which the beam eccentricity is taken into account but the beam stiffnesses are uniformly spread over the slab. The second set is a more realistic solution by GUSTAFSON

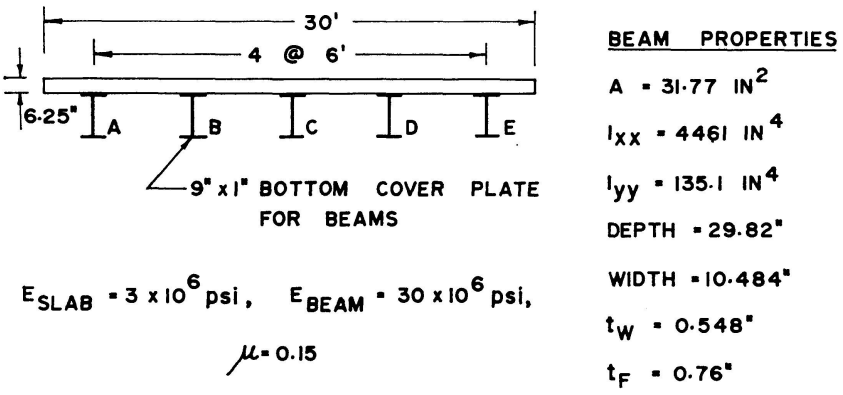

Fig. 6. Composite I-beam bridge. Example 1.

Table 2. Comparison of Moment Coefficients, C_m, for 60 ft. Span Composite I-Beam Bridge. Example 1

Basis of comparison	Load at midspan of	Moment at x	Beam A	Beam B	Beam C	Beam D	Beam E
Vitols et al. [8]	Beam A	$a/4$	0.0709	0.0625	0.0067	−0.0091	−0.0060
		$a/2$	0.1754	0.0870	0.0089	−0.0128	−0.0085
	Beam B	$a/4$	0.0364	0.0463	0.0354	0.0102	−0.0033
		$a/2$	0.0543	0.1324	0.0540	0.0139	−0.0046
	Beam C	$a/4$	0.0072	0.0353	0.0400		
		$a/2$	0.0097	0.0539	0.1228		
Finite element [5] (10×16 mesh)	Beam A	$a/4$	0.0875	0.0400	0.0066	−0.0042	−0.0047
		$a/2$	0.1951	0.0592	0.0085	−0.0058	−0.0066
	Beam B	$a/4$	0.0405	0.0412	0.0350	0.0122	−0.0037
		$a/2$	0.0598	0.1255	0.0536	0.0163	−0.0051
	Beam C	$a/4$	0.0070	0.0352	0.0408		
		$a/2$	0.0090	0.0540	0.1238		
Discrete energy ($R = 10^{10}$ ft) (16×8 mesh)	Beam A	$a/4$	0.0880	0.0403	0.0072	−0.0031	−0.0040
		$a/2$	0.1961	0.0607	0.0093	−0.0045	−0.0051
	Beam B	$a/4$	0.0405	0.0418	0.0351	0.0122	−0.0035
		$a/2$	0.0611	0.1255	0.0552	0.0169	−0.0044
	Beam C	$a/4$	0.0074	0.0354	0.0412		
		$a/2$	0.0096	0.0556	0.1242		

and Wright [5] using finite elements with a 10×16 mesh (10 radially and 16 circumferentially) for the bridge. In the present method the slab and beam forces are obtained separately and the stresses at the bottom of the beams are computed directly. In order to obtain the moment coefficients for comparison, the moment required to produce the computed stress at the bottom of the beam for a composite beam with 6 ft. wide slab is evaluated first. Table 2 shows that the values obtained by the discrete energy method compare very favourably with the finite element solutions and are everywhere on the higher side as expected. A 16×8 mesh (16 radially and 8 circumferentially) has been used in the present analysis for the full bridge.

Example 2: The second example is a perspex model of a curved slab-beam system experimentally investigated by AGRAWAL [9]. The details of the model are shown in Fig. 7. The straight edges of the model have simply supported

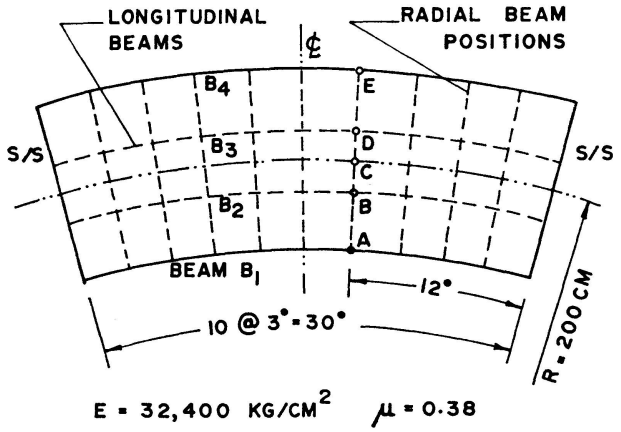

a) Plan

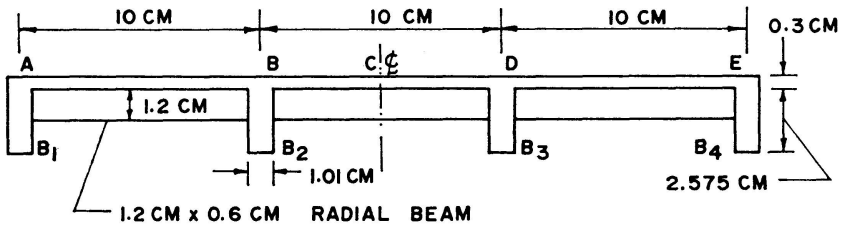

b) Section

Fig. 7. Curved slab beam system. Example 2.

conditions while the curved edges are free. Experimental values of deflections and strains are available for two set-ups: a) slab with longitudinal beams and no radial beams, and b) slab with both longitudinal and radial beams. In the present analysis a 10×10 mesh is used for discretizing the entire model. Tangential strains at mid-span at top of slab on the outer radius and at the bottom of the second and the outermost beams are compared with experimental values in Table 3. The values are for 10 kg load applied at the load positions shown in Fig. 7. When the load is at the inner radius, the experimentally recorded values of strain at the outer radius are very small and cannot therefore be taken for a reliable comparison. Where the strain values are significant, the theoretical and experimental values agree very well, the percentage difference being less than 5 per cent in most cases. The theoretical values are again on the higher side.

Example 3: The third example is another perspex model of a two span curved girder bridge with two longitudinal girders and a system of radial beams shown in Fig. 8. This model has been experimentally investigated by

Table 3. Comparison of Experimental and Theoretical Strains for Example 2 (see Fig. 7)

Load position	Strain at	Tangential strain at midspan, in micro-strain					
		without radial beams			with radial beams		
		Experiment	Theory	Difference as a percentage	Experiment	Theory	Difference as a percentage
A	B_2 bottom	930	938	0.89	870	907	4.25
	B_4 top	−10	−117	—	−11	−143	—
	B_4 bottom	94	211	—	140	250	—
B	B_2 bottom	1062	1089	2.54	760	800	5.26
	B_4 top	−335	−345	2.98	−330	−371	12.42
	B_4 bottom	594	608	2.35	732	787	7.51
C	B_2 bottom	795	807	1.51	732	742	1.36
	B_4 top	−470	−479	1.91	−468	−495	5.77
	B_4 bottom	906	943	4.08	1062	1095	3.11
D	B_2 bottom	527	563	6.83	634	684	7.88
	B_4 top	−590	−622	5.43	−592	−617	4.22
	B_4 bottom	1325	1386	4.60	1380	1421	2.97
E	B_2 bottom	284	321	13.03	513	511	−0.39
	B_4 top	−765	−823	7.58	−810	−822	1.48
	B_4 bottom	2160	2258	4.54	2060	2040	−0.97

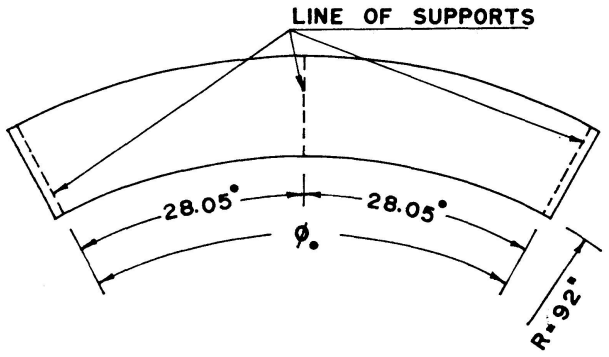

a) Plan

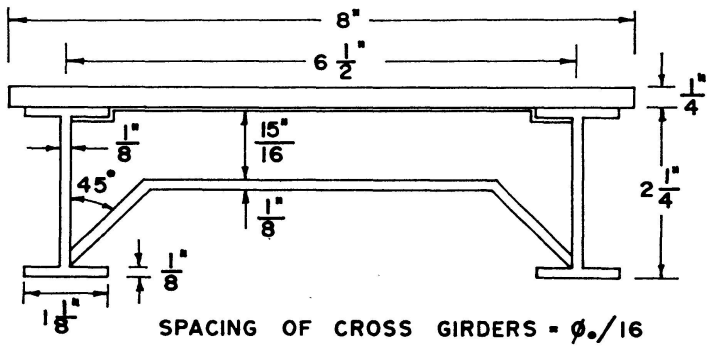

b) Cross section

Fig. 8. Two span curved girder bridge. Example 3.

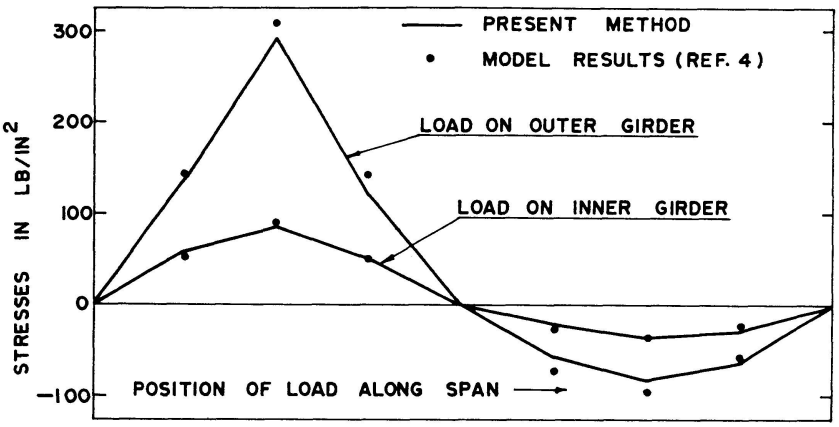

Fig. 9. Stresses at lower flange of outer girder. Example 3.

CULVER and CHRISTIANO [4] and experimental values of deflections and stresses are available. The comparison of average tangential stresses at the bottom of the outer girder due to a 15 lb. load at inner and outer girders at various positions along the span is shown in Fig. 9. Values of elastic constants and sectional properties used in the present analysis are obtained as far as possible from reference [4]. The comparison shows that the two sets of values agree well for load on the inner girder. For load on the outer girder, the stresses are underestimated by the present analysis for the two-span bridge. A 8×16 mesh (8 radially and 16 circumferentially) has been used for the entire bridge.

A general computer program has been developed on the CDC 3600 Computer system for analysis of structures by the present method. A block elimination scheme is used for the solution of the overall matrix equation assembled in half-band form.

4. Conclusions

A discrete energy formulation has been developed herein for the analysis of polar orthotropic sector plates with eccentric stiffeners placed radially and circumferentially. As seen from the results of the numerical examples, the method is suitable for curved slab-beam systems with arbitrary boundary conditions and loading including single and multi-span curved girder bridges. For slabs with closely and uniformly spaced radial beams of identical sections, the orthotropic plate formulation presented here may be used with a consequent reduction in the amount of numerical computations and the number of unknowns in the matrix equation. For radial beams with arbitrary spacing or sections, matrix formulations similar to that for the longitudinal beams can be used.

Computations required in the present method are less than in the finite element method since integrations in the element stiffness matrix formulation, which generally have to be evaluated numerically for curved finite elements,

are avoided. However, the method lacks the versatility of the finite element formulation with triangular elements, as it cannot be readily applied to slabs with irregular boundaries. In such cases, stepped boundaries have to be used to fit into the regular pattern. The formulation can also be modified for arbitrary mesh spacing so that a graded mesh can be used where required.

References

1. Sawko, F.: Computer analysis of grillages curved in plan. Publications, International Association for Bridge and Structural Engineering, Vol. 27, 1967, p. 171–186.
2. Heins, C. P., Jr., and Hails, R. L.: Behaviour of stiffened curved plate model. Proceedings of the American Society of Civil Engineers. Journal of the Structural Division, November 1969, Vol. 95, No. ST 11, Proceedings Paper 6876, p. 2353–2370.
3. Bell, L. C. and Heins, C. P.: Analysis of curved girder bridges. Proceedings of the American Society of Civil Engineers. Journal of the Structural Division, August 1970, Vol. 96, No. ST 8, Proceedings Paper 7462, p. 1657–1673.
4. Culver, C. P. and Christiano, P. D.: Static model test of curved girder bridge. Proceedings of the American Society of Civil Engineers. Journal of the Structural Division, August 1969, Vol. 95, No. ST 8, Proceedings Paper 6712, p. 1599–1614.
5. Gustafson, W. C. and Wright, R. N.: Analysis of skewed composite girder bridges. Proceedings of the American Society of Civil Engineers. Journal of the Structural Division, April 1968, Vol. 94, No. ST 4, Proceedings Paper 5890, p. 919–942.
6. Davies, J. D., Somervaille, I. J. and Zienkiewicz, O. C.: Analysis of various types of bridges by finite element method. Conference on "Development in bridge design and construction", University College, Cardiff, March 29–April 2, 1971.
7. Buragohain, D. N.: Discrete analysis of cylindrical orthotropic curved bridge decks. Publications, International Association for Bridge and Structural Engineering, Vol. 32, Part 1, 1972, p. 37–47.
8. Vitols, V., Clifton, R. J. and Au, T.: Analysis of composite beam bridges by orthotropic plate theory. Proceedings of the American Society of Civil Engineers. Journal of the Structural Division, August 1963, Vol. 89, No. ST 4, Proceedings Paper 3584, p. 71–94.
9. Agrawal, S. B.: Discrete analysis and model test of curved girder bridges. Dissertation submitted to the Department of Civil Engineering, Indian Institute of Technology, Bombay, in partial fulfilment of the requirements for the degree of Master of Technology, 1972.

Summary

A discrete energy formulation is presented for polar orthotropic curved slabs with eccentric radial and curved longitudinal beams. A modified finite difference scheme is used to discretize the slab separately into two sets of elements: Elements in extension and bending and elements in shear and twisting. The eccentric longitudinal beams are treated similarly. For closely spaced radial beams, an orthotropic plate formulation is used for the slab and radial beams taken together with due consideration of the beam eccentricity. Results for three numerical examples are presented.

Résumé

On présente une formulation d'énergie discrète pour des plaques courbes polaires et orthotropes avec poutres radiales et périphériques disposées excentriquement. On se sert d'une méthode modifiée de différences finies en vue de séparer la structure des plaques en deux genres d'éléments: éléments sous tension et flexion, et éléments sous cisaillement et torsion. Les poutres longitudinales excentriques sont traitées de manière similaire. Pour des poutres radiales disposées étroitement entre elles on se sert d'une formulation orthotrope pour l'ensemble des plaques et poutres radiales, en tenant compte de l'excentricité des poutres. Les résultats sont discutés par trois exemples numériques.

Zusammenfassung

Es wird eine diskrete Energieformulierung für polare orthotrope gekrümmte Platten mit exzentrisch radialen und peripheren Balken vorgelegt. Man bedient sich einer modifizierten finiten Differenzenmethode, um die Plattenstruktur in zwei Arten von Elementen zu trennen: Elemente unter Dehnung und Biegung, und Elemente unter Schub und Drehung. Die exzentrischen Längsträger werden ähnlich behandelt. Für eng aneinander liegende radiale Balken wird eine orthotrope Plattenformulierung für die Platten und die Radialbalken zusammen benutzt, unter Berücksichtigung der Balken-Exzentrizität. An drei Zahlenbeispielen werden die Ergebnisse erläutert.